



**HAL**  
open science

## 3D Hybrid Model of the Axial Flux Motor Accounting Magnet Shape

Théo Carpi, Yvan Lefèvre, Carole Hénaux, Jean-François Llibre, Dominique Harribey

► **To cite this version:**

Théo Carpi, Yvan Lefèvre, Carole Hénaux, Jean-François Llibre, Dominique Harribey. 3D Hybrid Model of the Axial Flux Motor Accounting Magnet Shape. IEEE Transactions on Magnetics, 2020, pp.1-1. 10.1109/TMAG.2019.2950892 . hal-03012944

**HAL Id: hal-03012944**

**<https://hal.science/hal-03012944>**

Submitted on 18 Nov 2020

**HAL** is a multi-disciplinary open access archive for the deposit and dissemination of scientific research documents, whether they are published or not. The documents may come from teaching and research institutions in France or abroad, or from public or private research centers.

L'archive ouverte pluridisciplinaire **HAL**, est destinée au dépôt et à la diffusion de documents scientifiques de niveau recherche, publiés ou non, émanant des établissements d'enseignement et de recherche français ou étrangers, des laboratoires publics ou privés.

# 3D Hybrid Model of the Axial Flux Motor Accounting Magnet Shape

T. Carpi, Y. Lefèvre, C. Hénaux, J.F. Llibre and D. Harribey

Laboratoire Plasma et Conversion d'Énergie (LAPLACE), University of Toulouse, CNRS, 31000 Toulouse, France

This paper presents a generalization of an analytical model of an axial flux permanent magnet machine to any magnet shape. It uses an existing model which computes the 3D magnetic flux density by the separation of variables and finite difference method. The original magnet shape is modified by adding a radial dependency to the Fourier series description of permanent magnets magnetization. The model is then developed for a general complex magnet shape. As an example, the model will be computed for a circular magnet shape and will be compared to a finite element analysis.

**Index Terms**— Axial flux, finite difference method, Fourier series, magnetic scalar potential, magnet shape, permanent magnet, separation of variables.

## I. INTRODUCTION

THE structures of Axial Flux Permanent Magnet (AFPM) machine structures are still under development [1]. Thus, modeling some of their particularities is becoming an issue. In axial flux surface mounted permanent magnet machines, permanent magnets are often considered as sector shaped magnets. However, others magnet shapes can be found in some AFPM structures [1], [2], [3]. Nevertheless, considering 3D analytical modeling, despite the variety of the methods used, only sector shaped magnets have been considered [4], [5], [6].

The method developed in [6] consists in a combined resolution with analytical and finite difference method (FDM). The resolution is based on the image method where the geometry is repeated infinitely in the axial direction [5]. This way, the problem can be described by a double Fourier series in the axial and angular directions. The Laplacian is then solved by separation of variables. However, Bessel functions given for the radial solutions are not chosen because of their complexity. Instead, the  $r$  dependent function is kept unknown and solved by a 1D FDM.

This model is adaptable to any magnets distributions thanks to the Fourier series description. It is also adaptable to multistage machines thanks to the image method. Nevertheless, only sector shaped magnets can be modeled by this method. Benefiting from the FDM in the radial direction, this paper proposes to extend the model to any magnet shapes by modifying the Fourier series description for each discretized radius. Subsequently, the solution will be computed for circular magnet shape and compared to finite element analysis (FEA).

## II. GENERALIZATION OF THE MAGNET SHAPE

A single sided AFPM machine with axially magnetized surface mounted permanent magnets is considered in this paper.

As in [6], the following assumptions are made:

- Because of the air-space between the magnets, we assume that the permeability of magnets and the air is the same and equal to  $\mu_0$ .
- Back-irons have infinite permeability so the boundary conditions (BC) at the planes  $z = 0$  and  $z = h_m + g$  is taken as

normal flux boundary conditions. Where  $g$  is the airgap width and  $h_m$  the permanent magnet width.

- The problem is limited in the radial direction with parallel flux boundary conditions on cylinders at  $r = R_0$  and  $r = R_1$ .

Using magnetic scalar potential formulation (MSP),  $\Omega$ , the partial differential equation to be solved is deduced from Maxwell equations:

$$\Delta\Omega = \text{div } \mathbf{M} \quad (1)$$

with  $\mathbf{M}$  the magnetization vector.

To reduce the number of regions to consider, the image method is used to replace the normal flux BC by a periodical extension in the axial direction [6]. This leads to a double Fourier series description of the magnetization of the permanent magnets in the azimuthal  $\theta$  and axial  $z$  directions.

A complex magnet shape is considered in Fig. 1. To be able to compute this magnet shape, the Fourier series description has to be modified depending on the radial position. The parameters necessary to characterize any shape are the arc pole  $\alpha_p$  and the phase  $\beta$  between the origin and the center position of the angular opening as shown in Fig. 1. Thus, a general Fourier series describing the magnetization  $M_z$  of any magnet shape can be expressed as follows.

$$M_z(r, \theta, z) = \sum_n \sum_k M_{nk}(r) \cos(np\theta + \beta(r)) \cos\left(\frac{k\pi}{\tau}z\right) \quad (2)$$

where  $p$  is the number of pole pairs,  $\tau = h_m + g$  is the half period of the magnetization in the  $z$ -direction.

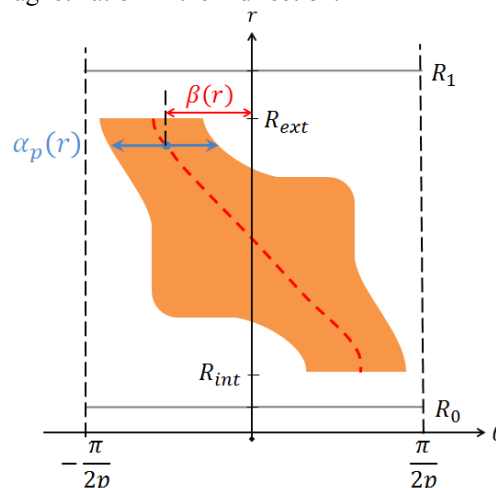


Fig. 1. Complex magnet shapes with the arc pole and the phase depending on radial position.

The coefficients  $M_{nk}$  have to be determined in function of  $\alpha_p(r)$  and the phase  $\beta(r)$  which represents purely the asymmetrical feature of the magnet shape. Fig. 2 shows the angular and axial dependency of the magnetization for a given radius. The image method repeats the geometry in the axial direction, so  $M_z(z)$  is not impacted by the magnet shape.

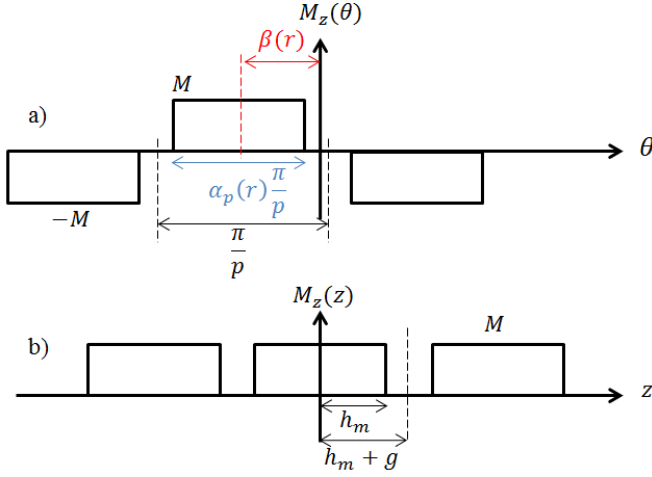


Fig. 2. Angular (a) and axial (b) dependency of the magnetization.

### III. HYBRID MODELING METHOD

Thanks to the double Fourier series description, there are three regions to be considered separated by cylindrical surfaces at  $r = R_{int}$  and  $r = R_{ext}$ . Air regions I ( $R_{int} \geq r \geq R_0$ ) and III ( $R_1 \geq r \geq R_{ext}$ ), and the PM region II ( $R_{ext} \geq r \geq R_{int}$ ). The new magnet shape must be included in the magnet region between  $R_{int}$  and  $R_{ext}$ .

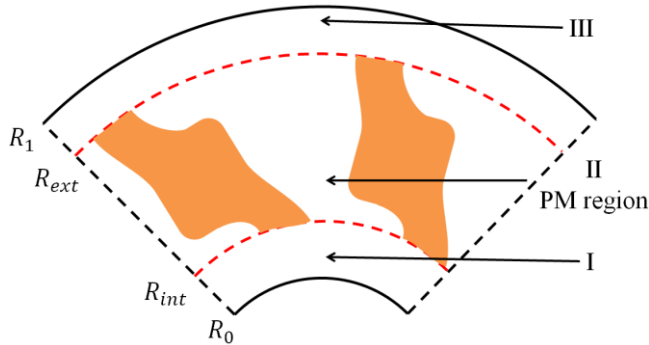


Fig. 3. Representation of the different regions considered in the problem.

In order to make the solution easier to handle, the Fourier series of the magnetization (2) is written in terms of cosine and sine functions.

$$M_z(r, \theta, z) = \sum_n \sum_k M_{c_{nk}}(r) \cos(np\theta) \cos\left(\frac{k\pi}{\tau} z\right) + \sum_n \sum_k M_{s_{nk}}(r) \sin(np\theta) \cos\left(\frac{k\pi}{\tau} z\right) \quad (3)$$

All the magnets are axially magnetized. Therefore, the magnetization  $\mathbf{M}$  has only a component in the axial direction. The second member of the equation (1) is reduced to:

$$\frac{\partial M_z}{\partial z} = \sum_n \sum_k -\frac{k\pi}{\tau} M_{c_{nk}}(r) \cos(np\theta) \sin\left(\frac{k\pi}{\tau} z\right) + \sum_n \sum_k -\frac{k\pi}{\tau} M_{s_{nk}}(r) \sin(np\theta) \sin\left(\frac{k\pi}{\tau} z\right) \quad (4)$$

The separation of variables consists in assuming that the solution  $\Omega$  is the product of three functions  $f$ ,  $g$  and  $h$ :

$$\Omega(r, \theta, z) = f(r) \cdot g(\theta) \cdot h(z) \quad (5)$$

Combining (1) and (5) leads to three ordinary differential equations for each function  $f$ ,  $g$  and  $h$ . The solutions for  $f$  are Bessel functions and cosine and sine functions both for  $h$  and  $g$ . To avoid using Bessel functions,  $f$  is kept unknown and will be determined by FD method. The principle of superposition allows writing the solution as follows:

$$\Omega(r, \theta, z) = \sum_n \sum_k \omega_{c_{nk}}(r) \cos(np\theta) \sin\left(\frac{k\pi}{\tau} z\right) + \sum_n \sum_k \omega_{s_{nk}}(r) \sin(np\theta) \sin\left(\frac{k\pi}{\tau} z\right) \quad (6)$$

The function  $f$  is now replaced by  $\omega_{c_{nk}}$  and  $\omega_{s_{nk}}$  which depend on the harmonic rank,  $np$  and  $k\pi/\tau$  are respectively the periodicities in the angular and axial direction. Thus, inserting (6) in the partial differential equation (1) yields to three ordinary differential equations in each region I, II and III over the new unknowns  $\omega_{c_{nk}}$  and  $\omega_{s_{nk}}$ .

$$\begin{cases} \frac{d^2 \omega_{c_{nk}}^I}{dr^2} + \frac{1}{r} \frac{d\omega_{c_{nk}}^I}{dr} - \left( \frac{k^2 \pi^2}{\tau^2} + \frac{n^2 p^2}{r^2} \right) \omega_{c_{nk}}^I = 0 \\ \frac{d^2 \omega_{c_{nk}}^{II}}{dr^2} + \frac{1}{r} \frac{d\omega_{c_{nk}}^{II}}{dr} - \left( \frac{k^2 \pi^2}{\tau^2} + \frac{n^2 p^2}{r^2} \right) \omega_{c_{nk}}^{II} = -M_{c_{nk}} \frac{k\pi}{\tau} \\ \frac{d^2 \omega_{c_{nk}}^{III}}{dr^2} + \frac{1}{r} \frac{d\omega_{c_{nk}}^{III}}{dr} - \left( \frac{k^2 \pi^2}{\tau^2} + \frac{n^2 p^2}{r^2} \right) \omega_{c_{nk}}^{III} = 0 \end{cases} \quad (7)$$

$$\begin{cases} \frac{d^2 \omega_{s_{nk}}^I}{dr^2} + \frac{1}{r} \frac{d\omega_{s_{nk}}^I}{dr} - \left( \frac{k^2 \pi^2}{\tau^2} + \frac{n^2 p^2}{r^2} \right) \omega_{s_{nk}}^I = 0 \\ \frac{d^2 \omega_{s_{nk}}^{II}}{dr^2} + \frac{1}{r} \frac{d\omega_{s_{nk}}^{II}}{dr} - \left( \frac{k^2 \pi^2}{\tau^2} + \frac{n^2 p^2}{r^2} \right) \omega_{s_{nk}}^{II} = -M_{s_{nk}} \frac{k\pi}{\tau} \\ \frac{d^2 \omega_{s_{nk}}^{III}}{dr^2} + \frac{1}{r} \frac{d\omega_{s_{nk}}^{III}}{dr} - \left( \frac{k^2 \pi^2}{\tau^2} + \frac{n^2 p^2}{r^2} \right) \omega_{s_{nk}}^{III} = 0 \end{cases} \quad (8)$$

There are  $n \times k$  equations to be solved in each region and for each cosine and sine component.

The boundary conditions (9) and (10) over the cylinders  $r = R_0$  and  $r = R_1$  are taken as parallel flux so that no flux goes out of the region:

$$B_r^I|_{r=R_0} = 0 \quad (9)$$

$$B_r^{III}|_{r=R_1} = 0 \quad (10)$$

The interface conditions (11) to (16) between the permanent magnet region II and the air regions (I and III) over the cylinders  $r = R_{int}$  and  $r = R_{ext}$  are the continuity of the normal component of the magnet flux density  $B_n$  and the continuity of the tangential component of the magnetic field density  $H_t$ :

$$B_r^I|_{r=R_{int}} = B_r^{II}|_{r=R_{int}} \quad (11)$$

$$H_\theta^I|_{r=R_{int}} = H_\theta^{II}|_{r=R_{int}} \quad (12)$$

$$H_z^I|_{r=R_{int}} = H_z^{II}|_{r=R_{int}} \quad (13)$$

$$B_r^I|_{r=R_{ext}} = B_r^{III}|_{r=R_{ext}} \quad (14)$$

$$H_\theta^I|_{r=R_{ext}} = H_\theta^{III}|_{r=R_{ext}} \quad (15)$$

$$H_z^I|_{r=R_{ext}} = H_z^{III}|_{r=R_{ext}} \quad (16)$$

Continuity of the tangential component of the magnetic field density  $H_t$  leads to the continuity of the functions  $\omega_{cnk}$  and  $\omega_{snk}$ , while the continuity of the normal component of the magnetic flux density  $B_r$  yields to the continuity of  $\partial\omega_{cnk}/\partial r$  and  $\partial\omega_{snk}/\partial r$ .

Adding the interface and boundary conditions bring about a matrix system for each harmonic rank gathering all equations mentioned before:

$$A_{cnk} \cdot v_{cnk} = B_{cnk} \quad (17)$$

$$A_{snk} \cdot v_{snk} = B_{snk} \quad (18)$$

The final expression of the axial magnetic flux density is deduced from the magnetic scalar potential solved by FD method:

$$B_z = -\mu_0 \left[ \sum_n \sum_k v_{cnk} \cdot \cos(np\theta) \cdot \frac{k\pi}{\tau} \cdot \cos\left(\frac{k\pi}{\tau} z\right) + \sum_n \sum_k v_{snk} \cdot \sin(np\theta) \cdot \frac{k\pi}{\tau} \cdot \cos\left(\frac{k\pi}{\tau} z\right) + M_z(r, \theta, z) \right] \quad (19)$$

where  $v_{nk}$  are functions of  $r$ . Differential equations are solved by FD method for each azimuthal  $n$  and axial  $k$  harmonics. The 1D FD method discretizes the problem in the radial direction and is continuous in the angular and axial directions thanks to the Fourier series description. The general method for any magnet shape was presented. In the next section, this model is applied to cylindrical magnet shape as an example.

#### IV. CIRCULAR MAGNET SHAPE

The model is applied to an AFPM machine with cylindrical magnets as shown in Fig. 4 and its parameters are given in Table 1. This magnet shape is often used in AFPM machines [1]. Thanks to the symmetrical shape of this type of magnet, the phase  $\beta(r)=0$  and the Fourier series of the magnetization  $M_z$  is reduced to (20).

$$M_z(r, \theta, z) = \sum_{n=1,3,5}^{\infty} \sum_{k=1}^{\infty} M_{nk}(r) \cos(np\theta) \cdot \cos\left(\frac{k\pi}{\tau} z\right) + \sum_{n=1,3,5}^{\infty} M_{n0}(r) \cos(np\theta) \quad (20)$$

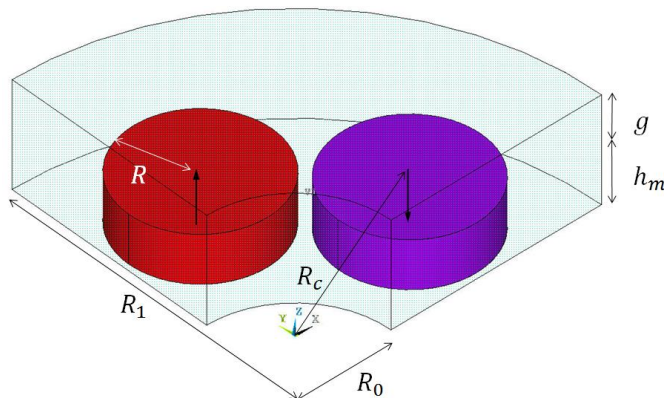


Fig. 4. 3-D view of the AFPM machine with circular magnets.

TABLE I  
PARAMETERS OF THE AFPM MACHINE

Parameter		Value
Magnetization (Remanence)	$M$ ( $B_r$ )	1.026 MA/m (1.29 T)
Magnet height	$h_m$	5 mm
Airgap height	$g$	6 mm
Minimum radius	$R_0$	10 mm
Maximum radius	$R_1$	32 mm
Magnet center radial position	$R_c$	21 mm
Magnets radius	$R$	7.5 mm
Pole pairs number	$p$	4

$M_{nk}$  and  $M_{n0}$  are the Fourier series coefficients:

$$M_{nk}(r) = \frac{8M}{nk\pi^2} \sin\left(k\pi \frac{h_m}{\tau}\right) \sin\left(\frac{n\alpha_p(r)\pi}{2}\right) \quad (21)$$

$$M_{n0}(r) = \frac{h_m 4M}{\tau n\pi} \sin\left(\frac{n\alpha_p(r)\pi}{2}\right) \quad (22)$$

For each discretized radius  $r$ , the arc pole is calculated in order to create a circular shape. The arc pole expression is deduced from Fig. 5 (a):

$$\alpha_p(r) = \left( \arccos \frac{R_c^2 + r^2 - R^2}{2R_c r} \right) / \frac{\pi}{2p} \quad (23)$$

As seen in Fig. 4,  $R_c$  is the radial position of the center of the magnet and  $R$  the radius of the circular magnet. This allows creating an exact circular shape from the initial sector shape. The arc pole function is plotted in Fig. 5 (b).

The FEA is carried out on ANSYS/Emag 3D [7] and based on a magnetic scalar potential formulation. The FEA is done under the same condition as the model, that means on one pair of poles of the machine. Also, the same assumptions are made: the permeability of the magnets and BC.

To validate the fact that the magnet shape has changed, both computation methods are compared on a radial line at the middle of the airgap  $z = h_m + g/2$  and for several angles  $\theta = 0^\circ$  (in front of the symmetrical axis),  $\theta = 5.5^\circ$  and  $\theta = 7.5^\circ$ .

The results are computed for 16 harmonics. The root mean square (RMS) error between the hybrid model and the FEA on Fig. 6 are about 1.2% for the three plots.

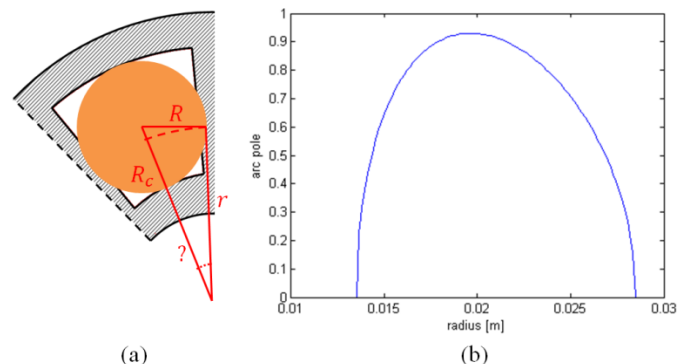


Fig. 5. Modification of magnets shape (a) and arc pole in function of the radius (b).

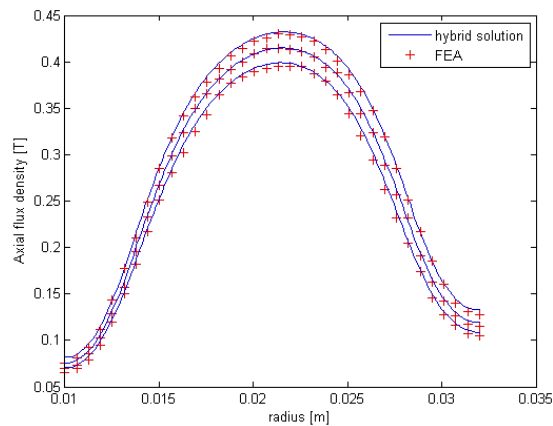


Fig. 6. Axial flux density as a function of the radial coordinate computed by hybrid analytical-FD method and FEA.

The RMS errors are about 1.2% and 0.6% if we consider the influence of  $\theta$  and  $z$  independently.

Back electromotive force and torque can be easily computed from the  $B_z$  component of the magnetic flux density [6]. If the field created by eddy currents may be neglected, eddy current losses in the magnets can be estimated. The armature reaction field must be computed. The laplacian can be solved in 2D ( $\theta, z$ ) using a MSP formulation [8]. Removing the magnets from this study and adding the boundary condition  $H_t = K$  at the interface with the stator ( $z = h_m + g$ ), where  $K$  is the current sheet modeling the winding distribution, allows to solve the problem. Then, the same method used to calculate eddy current losses in [8] can be applied.

## V. ACCURACY AND COMPUTATION TIME

The results of the hybrid model presented Fig. 6 are computed for 1) FDM part of the model: a radial discretization of 141 points and  $n$  and  $k$  equals 16 harmonics 2) analytical part of the model: 91 points and 221 points respectively for the angular and axial discretization. The total number of nodes is then 2,087,787 in the volume considered.

The computer used for the simulation is an Intel Core i7 at 1.9 GHz and 32 Go RAM. The computation time for 16 harmonics is 40 seconds to generate the entire solution. Nevertheless, the purpose here was to validate the model, so the computation time might be optimized. The addition of the radial dependency of the arc pole includes a loop into several initial nested loops, generating an increase of the computation time. It is approximately 4 times bigger than the one in [6], but remains much less than a FEA that took 74 seconds for 83,302 nodes within the same volume.

Fig. 7 presents the accuracy of the model and the computation time with respect to the number of harmonics. The RMS error mentioned above are the errors in the  $r$ -direction for  $z = h_m + g/2$  and  $\theta = 0$ ,  $\theta$ -direction for  $r = R_{int} + 0.8(R_{ext} - R_{int})$  and  $z = h_m + g/2$  and  $z$ -direction for  $r = R_{int} + 0.8(R_{ext} - R_{int})$  and  $\theta = 0$ . Therefore, a good accuracy can be reached with a small number of harmonics, and the computation time is convenient to include the model into optimization studies for example. Thus, this model presents the advantage of being faster, easy to set up, and offering larger perspectives over the usual FEA.

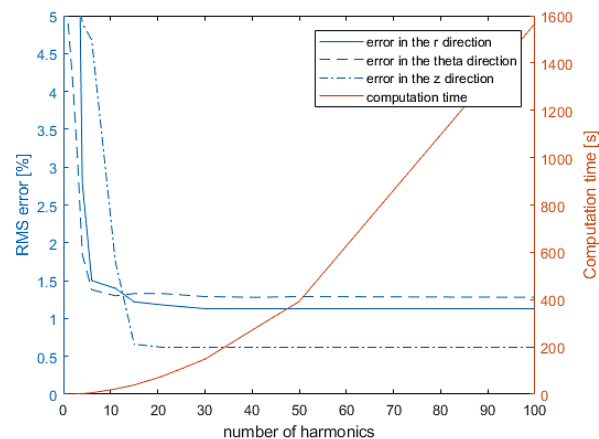


Fig. 7. Accuracy and computation time in function of the number of harmonics.

## VI. CONCLUSION

This paper presents a generalization of a 3D analytical model of AFPM with sector shaped magnets to AFPM with more complex magnet shapes. The method consists in including a radial dependency to the Fourier series description of the magnetization to be able to compute any magnets shape. The model was developed for a general complex magnet shape and the specific case of circular magnet shape was taken as an example, the method was validated by comparison with FEA.

The initial model is suitable to model a lot of particularities that can be found in axial flux machines such as multistage machines, different winding distributions and different magnets distributions. This paper extends the model to possibly any magnets shapes. Thus, this paper provides a method to model a lot of particularities of AFPM machines that usually require FEA. This allows further optimization studies over the magnet shape.

## VII. REFERENCES

- [1] M. Shokri, N. Rostami, V. Behjat, J. Pyrhönen, M. Rostami, "Comparison of performance characteristics of axial-flux permanent magnet synchronous machine with different magnet shapes", *IEEE Trans. Magn.*, vol. 51, December 2015.
- [2] M. R.A. Pahlavani, Y. S. Ayat, A. Vahedi, "Minimisation of torque ripple in slotless axial flux BLDC motors in terms of design considerations", *IET Electr. Power Appl.*, 2017, Vol. 11, Iss. 6, pp. 1124-1130.
- [3] M. Gulec, M. Aydin, "Magnet asymmetry in reduction of cogging torque for integer slot axial flux permanent magnet motors", *IET Electr. Power Appl.*, vol. 8, no. 5, pp. 189-198, 2014.
- [4] Y. Huang, B. Ge, J. Dong, H. Lin, J. Zhu, Y. Guo, "3-D analytical modeling of no-load magnetic field of ironless axial flux permanent magnet machine", *IEEE Trans. Magn.*, vol. 48, no. 11, pp. 2929-2932, Nov. 2012.
- [5] Ping Jin, Yue Yuan, Miyi Jin et al., "3-D analytical magnetic field analysis of axial flux permanent magnet machine", *IEEE Trans. Magn.*, vol. 50, no. 11, pp. 3504-3507, 2014.
- [6] T. Carpi, Y. Lefevre, C. Henaux, "Hybrid Modeling Method of Magnetic Field of Axial Flux Permanent Magnet Machine," *2018 XIII International Conference on Electrical Machines (ICEM)*, Alexandroupoli, Greece Sept. 2018.
- [7] ANSYS Mechanical APDL Low Frequency Electromagnetic Analysis 215 Guide. Release 17.2 documents, Aug. 2016.
- [8] A. Hemeida, P. Sergeant, "Analytical modeling of eddy current losses in Axial Flux PMSM using resistance network", *2014 Int. Conf. Electr. Mach. IEEE*, pp. 2688-2694, Sep 2014.